Hindawi
Wireless Communications and Mobile Computing
Volume 2021, Article ID 8865615, 11 pages
https://doi.org/10.1155/2021/8865615

Research Article

On the Capacity of Full-Duplex AF/DF Relay System with Energy Harvesting for Vehicle-to-Vehicle Communications

Ba Cao Nguyen[1], **Xuan Hung Le**[1], **Van Duan Nguyen**[1] and **Le The Dung**[2,3]

[1]*Telecommunications University, Khanh Hoa Province, Vietnam*
[2]*Division of Computational Physics, Institute for Computational Science, Ton Duc Thang University, Ho Chi Minh City, Vietnam*
[3]*Faculty of Electrical and Electronics Engineering, Ton Duc Thang University, Ho Chi Minh City, Vietnam*

Correspondence should be addressed to Le The Dung; lethedung@tdtu.edu.vn

Received 27 August 2020; Revised 7 November 2020; Accepted 2 December 2020; Published 4 February 2021

Academic Editor: Changqing Luo

This paper studies the ergodic capacity (EC) of full-duplex (FD) amplify-and-forward (AF) and decode-and-forward (DF) relay system with energy harvesting (EH) for vehicle-to-vehicle (V2V) communications. Unlike previous works on FD-EH systems, we consider the case that both relay and destination are mobile vehicles while the source is a static base station. We mathematically derive the exact closed-form expressions of ECs of both AF and DF protocols of the considered FD-EH-V2V relay system over cascade (double) Rayleigh fading. Our numerical results show that the ECs in the case of the V2V communication system are reduced compared to those in the case of stationary nodes. Also, with a specific value of residual self-interference (RSI), the ECs of the considered FD-EH-V2V relay system can be higher or lower than those of half-duplex- (HD-) EH-V2V system, depending on the average transmission power of the source. Furthermore, when the transmission power of the source and RSI are fixed, the ECs of the considered system can achieve peak values by using optimal EH time duration. On the other hand, the ECs of both AF and DF protocols reach the capacity floors in the high signal-to-noise ratio (SNR) regime due to the RSI impact. Also, the effect of RSI dominates the impact of cascade Rayleigh fading in the high SNR regime. Finally, we validate our analysis approach through Monte-Carlo simulations.

1. Introduction

In the age of Industry 4.0, various new techniques have been fast developed to satisfy the requirements of capacity and energy consumption of the future wireless networks such as the fifth-generation (5G) and beyond (B5G) [1–3]. In addition, the emergence of trillions of Internet-of-Things (IoT) devices in the world requires devices to consume less energy and transmit data at a higher rate [3, 4]. Therefore, energy harvesting (EH) from radio frequency (RF) signals has been used to deal with these issues [4, 5]. Together with the traditional energy grid, EH can help to fulfill the energy requirements for different elements of 5G networks, including sensors in the IoT, mobile devices, heterogeneous networks (HetNets), relays in device-to-device (D2D) systems, and computing servers [3]. Additionally, the emergence of advanced materials and hardware designs helps realize the EH circuits for small portable consumer electronic devices in the IoT. Furthermore, RF signals can be transmitted over the air all the time. Thus, EH from RF signals can provide stable energy for wireless devices that consume low power such as IoTs, sensors, and the remote area communication used in 5G and B5G systems [1, 3].

Meanwhile, full-duplex (FD) is a promising technique for achieving high spectral efficiency in wireless systems thanks to its capability to allocate the transmitted and received radio signals of a communication node on the same frequency and in the same time slot. Ideally, FD transmission increases the spectral efficiency twice compared to traditional half-duplex (HD) transmission. As a promising technology for next-generation (5G and B5G) wireless networks, FD wireless not only has the potential to double the spectrum efficiency in the physical layer but can also enhance the performance of wireless systems such as reducing feedback delay, end-to-end delay, and congestion, improving the network secrecy and efficiency and increasing the throughput and spectrum

usage flexibility [6, 7]. Overall, it is envisaged that FD communication technology can be adopted in the near future in a number of scenarios and applications, such as throughput enhancement in the sub-6 GHz band, supporting ultralow delay communication, small and dense cells [6, 8–10].

In the literature, various works have combined EH and FD techniques in a wireless communication system to solve the battery and spectrum efficiency issues [8, 10, 11]. The mathematical analysis and the experimental measurements have been applied for investigating the performance of FD-EH systems. Specifically, the mathematical analysis is used to derive expressions of outage probability (OP), symbol error rate (SER), bit error rate (BER), and ergodic capacity (EC) of the FD-EH systems [8, 10–13]. Based on these obtained mathematical expressions, the system behavior is analyzed under the effects of different parameters such as the residual self-interference (RSI) induced by FD transmission mode, the time switching ratio, and the channel conditions. It is found that optimal power allocation for FD transmission mode and optimal time switching ratio for EH can improve the system performance significantly [14–16]. Furthermore, the EC of the FD-EH system is generally higher than that of the HD-EH system for specific RSI values. Experimental measurements have also been widely used to evaluate the algorithms and solutions used to improve the performance of FD-EH systems [12, 17–19]. By applying the optimization problem in a nonconvex form, the FD-EH system's system power is minimized and better than that of the HD-EH system [19], and the sum rate and energy efficiency are maximized [18]. As a result, most of the works about FD-EH systems have analyzed RSI and other system parameters' impacts and then proposed solutions to reduce OP and SER and enhance EC and energy efficiency. Furthermore, exploiting FD-EH systems in different scenarios such as cognitive radio (CR), spatial modulation (SM), and cooperative communication has been widely carried out.

Recently, both FD and EH techniques are deployed in vehicle-to-vehicle (V2V) communication systems because of their various advantages in V2V environments. Thanks to FD and EH techniques, the V2V communication systems can reduce the delay time for signal transmission between vehicles and the power supply limitation problem [20, 21]. Hence, the FD-EH-V2V relay system can be applied for the intelligent transportation systems (ITS) and the road safety applications [8, 10, 20]. Specifically, the onboard unit was proposed in [20] to supply the energy for FD-V2V communications from the vehicle engine. Although this scheme could solve the energy issues, applying EH for V2V communication systems still becomes an inevitable trend thanks to many advantages of the EH technique. In recent reports, the OP, SER, and throughput of the FD-EH-V2V relay systems were obtained to investigate the system performance and evaluate the effects of several system parameters such as RSI, time switching ratio, and channel characteristics [8, 10]. In particular, papers [8, 10] derived the OP and SER expressions of FD-EH-V2V relay systems with AF and DF relaying protocols, respectively. However, the EC expressions of these FD-EH-V2V relay systems were not obtained. Meanwhile, we always want to get the lowest OP/SER and the highest EC for wireless communication systems. Therefore, investigating OP/SER and ignoring EC when analyzing the performance of wireless communication systems may result in inaccurate conclusions on the system behaviors. Specifically, experiments and measurements indicate that the cascade (double) Rayleigh fading distribution best describes the channels between vehicle nodes [21, 22], while the traditional channels such as Nakagami, Rician, and Rayleigh cannot fully model the V2V communication channel. It is shown that, under the effects of RSI and cascade Rayleigh fading channel, the OP and SER of the FD-EH-V2V relay systems reach the error floor faster in the high SNR regime. Additionally, the cascade Rayleigh fading channel makes the derivation of closed-form expressions more difficult than Nakagami, Rician, and Rayleigh channels [8, 10, 22], leading to a lack of mathematical analysis of FD-EH-V2V relay systems over cascade Rayleigh fading channels.

As in the above discussions, the main benefit of FD transmission is high capacity compared with HD one. However, mathematical analysis of the EC of FD-EH-V2V relay systems under the effect of cascade Rayleigh fading has not been investigated yet. Meanwhile, EH and FD techniques in V2V communication systems are inevitable because these techniques can solve various issues in traditional V2V systems. Mainly, EH is an effective method for power supply in the case that the wireline power supply may not be deployed for moving vehicles. At the same time, the FD can improve the performance of safety applications for V2V systems. Therefore, it is required to mathematically analyze the ECs of the FD-EH-V2V relay system for both AF and DF protocols to evaluate the system behavior. This observation motivates us to perform a mathematical analysis of the ECs of the FD-EH-V2V relay system with AF/DF protocols over cascade Rayleigh fading channels. In our paper, we focused on analyzing the impacts of the cascade Rayleigh fading channel, RSI, and time switching ratio on the ECs of the FD-EH-V2V relay system with the AF/DF protocol by deriving the exact closed-form expressions of these attributes and comparing with those in the case of Rayleigh fading channel, perfect SIC, and HD system. So far, this is the first work deriving the EC expressions of the FD-EH-V2V relay system over cascade Rayleigh fading channels. It is noted that exploiting EH from RF signals provides a stable energy supply for low-power consumption networks such as IoTs, wireless sensor networks, extremely remote area communications used in 5G and B5G systems [4, 19], and vehicular networks [23]. Meanwhile, FD transmission mode can be exploited in various scenarios to support a set of safety applications in V2V systems because FD devices can transmit signals and sense the environment simultaneously, thus reducing the end-to-end delay of the systems [6]. Consequently, the combination of EH and FD in a V2V system can achieve many advantages such as solving the battery and spectrum efficiency issues. The main contributions of the paper are shortened as follows:

(i) We investigate an FD-EH-V2V relay system where the source is located at a fixed location while relay and destination move on the road. Besides, relay

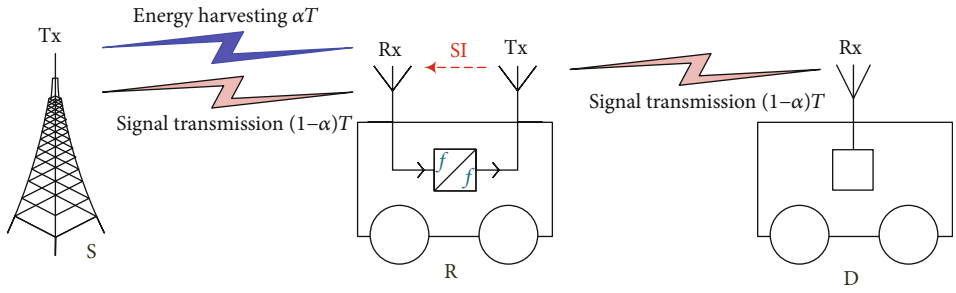

Figure 1: Block diagram of the considered FD-EH-V2V relay system.

harvests energy from the source while moving and exchanging signals. Furthermore, we consider both AF and DF protocols at the relay

(ii) We mathematically derive the exact closed-form expressions of the ECs of the considered FD-EH-V2V relay system for both AF and DF protocols under the influences of RSI and cascade Rayleigh fading, then validate these derived expressions by Monte-Carlo simulations. We also observe that cascade Rayleigh fading results in more difficulties deriving closed-form expression than traditional channels such as Rayleigh and Nakagami

(iii) We investigate the performance of the FD-EH-V2V relay system in different scenarios. Numerical results reveal that the cascade Rayleigh fading hurts the ECs of the considered system compared with the Rayleigh fading. Furthermore, the EC of the DF protocol is higher than that of AF one, and the ECs of the considered system are higher than those of the HD-EH-V2V relay system for certain RSI and SNR. On the other hand, when RSI and the average transmission power of the source are fixed, a suitable time switching ratio can be chosen to maximize the ECs of the considered system

The rest of the paper is organized as follows. Section 2 describes the system model of the considered FD-EH-V2V relay system with signal processing for both AF and DF protocols. Section 3 mathematically derives the EC expressions of the considered system. Section 4 provides numerical results and discussions. Finally, Section 5 draws some conclusions.

2. System Model

The considered FD-EH-V2V relay system consists of a static station (S) and two moving vehicles (R and D), as described in Figure 1. S and D are equipped with one antenna while R is equipped with two antennas, one for receiving and another for transmitting signals. S and D use traditional HD communication, while R employs FD communication. When R is moving on the road or restricted area, it is not easy to supply power to it; thus, R needs to harvest energy from RF signals for its operation. In particular, R is equipped with a suitable circuit that can harvest energy from the RF signal transmitted from S and then uses all the harvested energy for signal transmission. In practice, R can use a shared antenna for both transmitting and receiving signals; however, exploiting a separate antenna can suppress self-interference (SI) better, especially in the propagation domain. Specifically, when a shared antenna is exploited at R, the isolation between its output and input may not be sufficient to satisfy the SIC requirements [24, 25]. Additionally, it is too difficult to apply the spatial suppression at R with a shared antenna. Meanwhile, various methods to suppress SI power with a separate antenna such as the usage of lossy materials, directional antennas, and spatial suppression can be easily deployed [25, 26]. Hence, R keeps antennas separately on the vehicle rooftop to perform this task at a far enough distance to make passive isolation remarkably efficient. In this paper, we also assume that R uses two separate antennas.

As can be seen from Figure 1, besides the signal processing as traditional AF/DF relay, the relay in the considered system has to deal with EH and SIC processes. In addition, various algorithms to suppress the SI are also exploited at the EH-FD relay. These operations lead to an increase in the architecture complexity and signal processing delay at the relay. Therefore, the considered FD-EH-V2V relay system is more complex than the traditional HD relay system without EH [27, 28]. On the other hand, the transmission delay was characterized in several papers such as [29–31]. Since the authors of [29–31] analyzed a two-hop HD relay system, the data transmitted from source to destination via relay needs two time slots, leading to a significant increase in the signal transmission delay. In contrast, there is only one time slot for transmitting data from source to destination in our work because of FD transmission mode. Thus, the delay is greatly reduced. Furthermore, we focus on the mathematical analysis of the ergodic capacity (EC) of the V2V relay system with two new techniques (EH and FD) and both amplify-and-forward (AF) and decode-and-forward (DF) relaying protocols by deriving the closed-form EC expressions. Then, we compare the ECs of the considered system with ECs of the traditional HD system or the system over Rayleigh fading to exhaustively investigate the impacts of cascade Rayleigh fading channel, RSI, and the benefits of FD transmission mode. In the near future, we will extend this work by analyzing the scenario where the delay is considered in FD-V2V relay systems.

The operation of the considered FD-EH-V2V relay system is illustrated in Figure 2. It consists of two stages. In the first stage, R harvests the energy from the RF signal transmitted from S in the time duration of αT, where $0 \leq \alpha \leq 1$ and

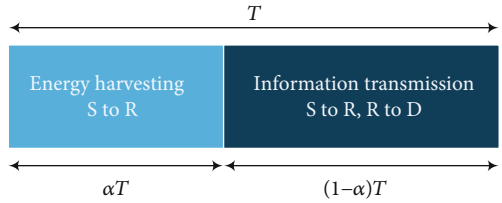

Figure 2: The operation of the considered FD-EH-V2V relay system with the TS protocol.

T are, respectively, the time switching ratio and the transmission block. In the second stage, S and R transmit signals to R and D, respectively, in the time duration of $(1-\alpha)T$. Due to simultaneously transmitting and receiving at the same time and same frequency band, the received signal at R is distorted by the SI. Thus, all SIC techniques should be applied at R to mitigate this issue.

Also, the measurements and experiments in the literature such as [32, 33] indicated that the well-known channels such as Nakagami-m, Rayleigh, and Rician do not fit the R–D communication channel. It is because both R and D are moving vehicles. Instead, the cascade Rayleigh fading well characterizes the R–D communication channel in both fields of measurement and theoretical analysis [22, 32, 33]. Meanwhile, since S is static, the S–R communication link follows Rayleigh fading [32, 34, 35].

In the EH time duration αT, the harvested energy at R (denoted by E_h) is expressed as

$$E_h = \eta\alpha T P_S |h_{SR}|^2, \tag{1}$$

where $0 \le \eta \le 1$ is the energy conversion efficiency; P_S is the average transmission power of S; h_{SR} is the fading coefficient of the S–R channel.

Then, R uses all the harvested energy for signal transmission. Consequently, the transmission power of R is given by

$$P_R = \frac{\eta\alpha T P_S |h_{SR}|^2}{(1-\alpha)T} = \frac{\eta\alpha P_S |h_{SR}|^2}{1-\alpha}. \tag{2}$$

In the communication time, $(1-\alpha)T$, S and R, respectively, transmit signals to R and D. Simultaneously transmitting and receiving signals of R causes SI from its transmitting antenna to its receiving antenna. The received signals at R is thus presented as

$$y_R = h_{SR}\sqrt{P_S}x_S + \tilde{h}_{RR}\sqrt{P_R}x_R + z_R, \tag{3}$$

where x_S and x_R are the transmitted signals at S and R, respectively; P_R is the transmission power of R given in (2); $\tilde{h}_{RR}$ is the fading coefficient of SI channel; z_R is the Gaussian noise at R with zero mean and variance of σ_R^2, i.e., $z_R \sim \mathcal{CN}(0, \sigma_R^2)$.

Since the distance between transmission and reception antennas of R is very small, especially for personal devices, R must apply all SIC techniques to suppress SI power before performing further processes such as decoding and forwarding. The average SI power before SIC from (3) is calculated as

$$\mathbb{E}\left\{\left|\tilde{h}_{RR}\right|^2 P_R\right\} = \frac{\eta\alpha P_S}{1-\alpha}\mathbb{E}\left\{\left|\tilde{h}_{RR}\right|^2 |h_{SR}|^2\right\}, \tag{4}$$

where $\mathbb{E}\{.\}$ denotes the expectation operator.

First, in the propagation domain, R uses antenna directionality, isolation, and cross-polarization to reduce the SI power. Then, through circuits and algorithms in both analog and digital domains, the SI is further suppressed. In particular, since R knows its transmitted signal, it can subtract this signal from the received signals, especially by using digital cancellation. However, due to imperfect circuit hardware and SI channel estimation, the SI cannot be obliterated. Therefore, residual self-interference (RSI) still exists in the received signals of R. According to the measurements and experiments on the RSI of FD devices, the RSI after using all SIC techniques (denoted by I_R) follows complex Gaussian distribution with zero mean and variance of σ_{RSI}^2 [15, 16, 36–38], where σ_{RSI}^2 is expressed as

$$\sigma_{RSI}^2 = \frac{k\eta\alpha P_S}{1-\alpha}, \tag{5}$$

where k is the RSI level at FD relay.

Now, the received signals at R becomes

$$y_R = h_{SR}\sqrt{P_S}x_S + I_R + z_R. \tag{6}$$

2.1. Amplify-and-Forward (AF). When R uses the AF protocol, it amplifies the received signals after SIC and forwards them to D. The transmitted signal at R is expressed as

$$x_R = G y_R, \tag{7}$$

where G is the relaying gain chosen so that $\mathbb{E}\{|x_R|^2\} = 1$, i.e.,

$$G = \sqrt{\frac{1}{|h_{SR}|^2 P_S + \sigma_{RSI}^2 + \sigma_R^2}}. \tag{8}$$

Then, R forwards signals to D. The received signal at D is presented as

$$y_D = h_{RD}\sqrt{P_R}x_R + z_D, \tag{9}$$

where h_{RD} is the fading coefficient of the R–D channel; z_D is the Gaussian noise at D, i.e., $z_D \sim \mathcal{CN}(0, \sigma_D^2)$.

Replacing (6), (7), and (8) into (9), we have

$$\begin{aligned} y_D &= h_{RD}\sqrt{P_R}G\left(h_{SR}\sqrt{P_S}x_S + I_R + z_R\right) + z_D \\ &= h_{SR}h_{RD}\sqrt{P_S}\sqrt{P_R}Gx_S + h_{RD}\sqrt{P_R}G(I_R + z_R) + z_D. \end{aligned} \tag{10}$$

From (10), the end-to-end signal-to-interference-plus-noise ratio (SINR) of the considered FD-EH-V2V relay system with the AF protocol (denoted by γ_{AF}) is computed as

$$\gamma_{\mathrm{AF}} = \frac{|h_{\mathrm{SR}}|^2 |h_{\mathrm{RD}}|^2 P_{\mathrm{S}} P_{\mathrm{R}} G^2}{|h_{\mathrm{RD}}|^2 P_{\mathrm{R}} G^2 \left(\sigma_{\mathrm{RSI}}^2 + \sigma_{\mathrm{R}}^2\right) + \sigma_{\mathrm{D}}^2}. \tag{11}$$

Substituting (2) and (8) into (11), γ_{AF} now becomes

$$\gamma_{\mathrm{AF}} = \frac{|h_{\mathrm{SR}}|^4 |h_{\mathrm{RD}}|^2 \eta\alpha P_{\mathrm{S}}^2}{|h_{\mathrm{SR}}|^2 |h_{\mathrm{RD}}|^2 \eta\alpha P_{\mathrm{S}} \left(\sigma_{\mathrm{RSI}}^2 + \sigma_{\mathrm{R}}^2\right) + \sigma_{\mathrm{D}}^2 (1-\alpha) \left(|h_{\mathrm{SR}}|^2 P_{\mathrm{S}} + \sigma_{\mathrm{RSI}}^2 + \sigma_{\mathrm{R}}^2\right)}. \tag{12}$$

2.2. Decode-and-Forward (DF). When R uses the DF protocol, it decodes the received signals after SIC, recodes the intended signals, and forwards them to D. The received signals at D is given in (9). Based on the received signals at R and D given as (6) and (9), the SINRs for decoding signals at R (denoted by γ_{R}) and D (denoted by γ_{D}) are, respectively, calculated as

$$\gamma_{\mathrm{R}} = \frac{|h_{\mathrm{SR}}|^2 P_{\mathrm{S}}}{\sigma_{\mathrm{RSI}}^2 + \sigma_{\mathrm{R}}^2}, \tag{13}$$

$$\gamma_{\mathrm{D}} = \frac{|h_{\mathrm{RD}}|^2 P_{\mathrm{R}}}{\sigma_{\mathrm{D}}^2} = \frac{|h_{\mathrm{SR}}|^2 |h_{\mathrm{RD}}|^2 \eta\alpha P_{\mathrm{S}}}{\sigma_{\mathrm{D}}^2 (1-\alpha)}. \tag{14}$$

For the DF protocol, the end-to-end SINR (denoted by γ_{DF}) of the considered FD-EH-V2V relay system is given by

$$\gamma_{\mathrm{DF}} = \min\left(\gamma_{\mathrm{R}}, \gamma_{\mathrm{D}}\right). \tag{15}$$

3. Performance Analysis

In this section, the ECs of the considered FD-EH-V2V relay system for both AF and DF protocols are obtained. Generally, the EC is computed as

$$\mathscr{C} = \mathbb{E}\{\log_2(1+\gamma_{\mathrm{e2e}})\} = \int_0^\infty \log_2(1+\gamma_{\mathrm{e2e}}) f_{\gamma_{\mathrm{e2e}}}(\gamma) d\gamma, \tag{16}$$

where γ_{e2e} is the end-to-end SINR of the considered system given in (12) and (15) for AF and DF protocols, respectively; $f_{\gamma_{\mathrm{e2e}}}(\gamma)$ is the probability density function (PDF) of γ_{e2e}.

After some mathematical manipulations, (16) becomes

$$\mathscr{C} = \frac{1}{\ln 2} \int_0^\infty \frac{1 - F_{\gamma_{\mathrm{e2e}}}(x)}{1+x} dx, \tag{17}$$

where $F_{\gamma_{\mathrm{e2e}}}(x)$ is the cumulative distribution function (CDF) of γ_{e2e}.

From (17), the ECs of the considered FD-EH-V2V relay system for both AF and DF protocols are derived in the following theorem.

Theorem 1. *Under the impacts of RSI and the cascade Rayleigh fading channels, the ECs of the considered FD-EH-V2V relay system using AF (denoted by $\mathscr{C}_{AF}$) and DF (denoted by $\mathscr{C}_{DF}$) protocols are expressed as*

$$\mathscr{C}_{AF} = \frac{\pi^2}{4MN \ln 2} \sum_{m=1}^{M} \sum_{n=1}^{N} \frac{\sqrt{\left(1-\phi_m^2\right)\left(1-\phi_n^2\right)}}{\Psi - \ln \nu} \cdot \sqrt{\frac{\Phi \ln \nu (\ln u + \ln \nu - \Psi)}{\Psi \ln u (\ln u + \ln \nu)}} K_1 \cdot \left(\sqrt{\frac{\Phi \ln \nu (\ln u + \ln \nu - \Psi)}{\Psi \ln u (\ln u + \ln \nu)}}\right), \tag{18}$$

$$\mathscr{C}_{DF} = \frac{\pi^2}{4MN \ln 2} \sum_{m=1}^{M} \sum_{n=1}^{N} \frac{\sqrt{\left(1-\phi_m^2\right)\left(1-\phi_n^2\right)}}{\Psi - \ln \nu} \cdot \sqrt{\frac{\Phi \ln \nu}{\Psi \ln u (\ln u + \ln \nu)}} K_1 \left(\sqrt{\frac{\Phi \ln \nu}{\Psi \ln u (\ln u + \ln \nu)}}\right), \tag{19}$$

where $\Psi = (\sigma_{RSI}^2 + \sigma_R^2)/P_S$; $\Phi = (4\sigma_D^2(1-\alpha))/\eta\alpha P_S$; $\phi_m = \cos(((2m-1)\pi)/2M)$; $u = 1/2(\phi_m + 1)$; $\phi_n = \cos(((2n-1)\pi)/2N)$; $\nu = 1/2(\phi_n + 1)$; *M and N are complexity-accuracy trade-off parameters [39];* $K_1(.)$ *is the first order modified Bessel function of the second kind [40].*

Proof. To obtain ECs for both cases of AF and DF protocols, we have to derive the CDFs of γ_{AF} and γ_{DF} first and then replace them into (17).

For the AF protocol, the CDF of γ_{AF} (denoted by $F_{\mathrm{AF}}(x)$) is computed as

$$\begin{aligned} F_{\mathrm{AF}}(x) &= \Pr\{\gamma_{\mathrm{AF}} < x\} \\ &= \Pr\left\{\frac{|h_{\mathrm{SR}}|^4 |h_{\mathrm{RD}}|^2 \eta\alpha P_{\mathrm{S}}^2}{|h_{\mathrm{SR}}|^2 |h_{\mathrm{RD}}|^2 \eta\alpha P_{\mathrm{S}} \left(\sigma_{\mathrm{RSI}}^2 + \sigma_{\mathrm{R}}^2\right) + \sigma_{\mathrm{D}}^2 (1-\alpha) \left(|h_{\mathrm{SR}}|^2 P_{\mathrm{S}} + \sigma_{\mathrm{RSI}}^2 + \sigma_{\mathrm{R}}^2\right)} < x\right\} \\ &= \Pr\left\{|h_{\mathrm{SR}}|^2 |h_{\mathrm{RD}}|^2 \eta\alpha P_{\mathrm{S}} \left[|h_{\mathrm{SR}}|^2 P_{\mathrm{S}} - x\left(\sigma_{\mathrm{RSI}}^2 + \sigma_{\mathrm{R}}^2\right)\right] < x\sigma_{\mathrm{D}}^2 (1-\alpha) \cdot \left(|h_{\mathrm{SR}}|^2 P_{\mathrm{S}} + \sigma_{\mathrm{RSI}}^2 + \sigma_{\mathrm{R}}^2\right)\right\}. \end{aligned} \tag{20}$$

By changing variable, i.e., $|h_{\mathrm{SR}}|^2 = y + (x(\sigma_{\mathrm{RSI}}^2 + \sigma_{\mathrm{R}}^2)/P_{\mathrm{S}})$, (20) becomes

$$\begin{aligned} F_{\mathrm{AF}}(x) &= \Pr\left\{|h_{\mathrm{RD}}|^2 < \frac{\sigma_{\mathrm{D}}^2 (1-\alpha) \left[\left(\sigma_{\mathrm{RSI}}^2 + \sigma_{\mathrm{R}}^2\right)\left(x^2 + x\right) + P_{\mathrm{S}} yx\right]}{\eta\alpha P_{\mathrm{S}} y \left[P_{\mathrm{S}} y + \left(\sigma_{\mathrm{RSI}}^2 + \sigma_{\mathrm{R}}^2\right) x\right]}\right\} \\ &= 1 - \int_0^\infty \left[1 - F_{|h_{\mathrm{RD}}|^2}\left(\frac{\sigma_{\mathrm{D}}^2 (1-\alpha) \left[\left(\sigma_{\mathrm{RSI}}^2 + \sigma_{\mathrm{R}}^2\right)\left(x^2 + x\right) + P_{\mathrm{S}} yx\right]}{\eta\alpha P_{\mathrm{S}} y \left[P_{\mathrm{S}} y + \left(\sigma_{\mathrm{RSI}}^2 + \sigma_{\mathrm{R}}^2\right) x\right]}\right)\right] \cdot f_{|h_{\mathrm{SR}}|^2}\left(y + \frac{x\left(\sigma_{\mathrm{RSI}}^2 + \sigma_{\mathrm{R}}^2\right)}{P_{\mathrm{S}}}\right) dy. \end{aligned} \tag{21}$$

To calculate (21), we begin with the CDF and PDF of the instantaneous channel gain, $|h_{\mathrm{SR}}|^2$, that follows Rayleigh distribution, i.e.,

$$F_{|h_{\mathrm{SR}}|^2}(x) = 1 - \exp\left(-\frac{x}{\Omega}\right), x \geq 0, \tag{22}$$

$$f_{|h_{\mathrm{SR}}|^2}(x) = \frac{1}{\Omega}\exp\left(-\frac{x}{\Omega}\right), x \geq 0, \tag{23}$$

where $\Omega = \mathbb{E}\{|h|^2\}$ is the average channel gain.

To shorten the derived expressions, all the average channel gains are normalized, i.e., $\Omega = 1$. Therefore, (22) and (23) become

$$F_{|h_{\mathrm{SR}}|^2}(x) = 1 - \exp(-x), x \geq 0, \tag{24}$$

$$f_{|h_{\mathrm{SR}}|^2}(x) = \exp(-x), x \geq 0. \tag{25}$$

In addition, since the R–D channel is influenced by cascade Rayleigh fading, the CDF and PDF of $|h_{\mathrm{RD}}|^2$ are, respectively, expressed as [22, 34, 41]

$$F_{|h_{\mathrm{RD}}|^2}(x) = 1 - \sqrt{4x}K_1\left(\sqrt{4x}\right), \tag{26}$$

$$f_{|h_{\mathrm{RD}}|^2}(x) = 2K_0\left(\sqrt{4x}\right), \tag{27}$$

where $K_0(.)$ is the zero-order modified Bessel function of the second kind [40].

It should be better to know that the movements of both transmitter and receiver make the signal's amplitude and phase fluctuate and cause the Doppler shifts. As a result, the cascade Rayleigh fading channels are widely used in V2V communication systems such as in [22, 35, 42] to best describe the characteristics of V2V channels. Through mathematical analysis, previous works such as [22, 33, 35, 43] take these characteristics into account when deriving the CDF and PDF of the V2V communication channels. In other words, the CDF in (26) and the PDF in (27) implicitly reflect the movements of both transmitter and receiver in the V2V system.

Applying (26) and (25), (21) becomes

$$\begin{aligned} F_{\mathrm{AF}}(x) = 1 - \int_0^\infty & \sqrt{\frac{4\sigma_{\mathrm{D}}^2(1-\alpha)\left[\left(\sigma_{\mathrm{RSI}}^2+\sigma_{\mathrm{R}}^2\right)(x^2+x)+P_{\mathrm{S}}yx\right]}{\eta\alpha P_{\mathrm{S}}y\left[P_{\mathrm{S}}y+\left(\sigma_{\mathrm{RSI}}^2+\sigma_{\mathrm{R}}^2\right)x\right]}} \\ & \times K_1\left(\sqrt{\frac{4\sigma_{\mathrm{D}}^2(1-\alpha)\left[\left(\sigma_{\mathrm{RSI}}^2+\sigma_{\mathrm{R}}^2\right)(x^2+x)+P_{\mathrm{S}}yx\right]}{\eta\alpha P_{\mathrm{S}}y\left[P_{\mathrm{S}}y+\left(\sigma_{\mathrm{RSI}}^2+\sigma_{\mathrm{R}}^2\right)x\right]}}\right) \\ & \cdot \exp\left(-y-\frac{x\left(\sigma_{\mathrm{RSI}}^2+\sigma_{\mathrm{R}}^2\right)}{P_{\mathrm{S}}}\right)dy. \end{aligned} \tag{28}$$

Let $z = \exp(-y)$ be a new variable, we can rewrite (28) as

$$\begin{aligned} F_{\mathrm{AF}}(x) = 1 - \exp & \left(-\frac{x\left(\sigma_{\mathrm{RSI}}^2+\sigma_{\mathrm{R}}^2\right)}{P_{\mathrm{S}}}\right)\int_0^1 \\ & \cdot \sqrt{\frac{4\sigma_{\mathrm{D}}^2(1-\alpha)\left[\left(\sigma_{\mathrm{RSI}}^2+\sigma_{\mathrm{R}}^2\right)(x^2+x)+P_{\mathrm{S}}x\ln(1/z)\right]}{\eta\alpha P_{\mathrm{S}}\left[P_{\mathrm{S}}\ln(1/z)+\left(\sigma_{\mathrm{RSI}}^2+\sigma_{\mathrm{R}}^2\right)x\right]\ln(1/z)}} \\ & \times K_1\left(\sqrt{\frac{4\sigma_{\mathrm{D}}^2(1-\alpha)\left[\left(\sigma_{\mathrm{RSI}}^2+\sigma_{\mathrm{R}}^2\right)(x^2+x)+P_{\mathrm{S}}x\ln(1/z)\right]}{\eta\alpha P_{\mathrm{S}}\left[P_{\mathrm{S}}\ln(1/z)+\left(\sigma_{\mathrm{RSI}}^2+\sigma_{\mathrm{R}}^2\right)x\right]\ln(1/z)}}\right) \\ & \cdot dz = 1 - \exp(-\Psi x)\int_0^1 \sqrt{\frac{\Phi[\Psi(x^2+x)+x\ln(1/z)]}{(\ln(1/z)+\Psi x)\ln(1/z)}}K_1 \\ & \cdot \left(\sqrt{\frac{\Phi[\Psi(x^2+x)+x\ln(1/z)]}{(\ln(1/z)+\Psi x)\ln(1/z)}}\right)dz. \end{aligned} \tag{29}$$

Using [39] (Eq. (25.4.30)), (29) is computed as

$$\begin{aligned} & \int_0^1 \sqrt{\frac{\Phi[\Psi(x^2+x)+x\ln(1/z)]}{(\ln(1/z)+\Psi x)\ln(1/z)}}K_1\left(\sqrt{\frac{\Phi[\Psi(x^2+x)+x\ln(1/z)]}{(\ln(1/z)+\Psi x)\ln(1/z)}}\right)dz \\ & = \frac{\pi}{2M}\sum_{m=1}^{M}\sqrt{1-\phi_m^2}\sqrt{\frac{\Phi[\Psi(x^2+x)-x\ln u]}{-\ln u(-\ln u+\Psi x)}}K_1 \\ & \cdot \left(\sqrt{\frac{\Phi[\Psi(x^2+x)-x\ln u]}{-\ln u(-\ln u+\Psi x)}}\right), \end{aligned} \tag{30}$$

where M, ϕ_m, and u were defined in the theorem.

Then, $F_{\mathrm{AF}}(x)$ is expressed as

$$\begin{aligned} F_{\mathrm{AF}}(x) = 1 - \exp(-\Psi x)\frac{\pi}{2M}\sum_{m=1}^{M}\sqrt{1-\phi_m^2}\sqrt{\frac{\Phi[\Psi(x^2+x)-x\ln u]}{-\ln u(-\ln u+\Psi x)}}K_1 \\ \cdot \left(\sqrt{\frac{\Phi[\Psi(x^2+x)-x\ln u]}{-\ln u(-\ln u+\Psi x)}}\right). \end{aligned} \tag{31}$$

Substituting $F_{\mathrm{AF}}(x)$ in (31) into (17) for calculating the EC corresponding to the AF protocol, we have

$$\begin{aligned} \mathscr{C}_{\mathrm{AF}} = \frac{1}{\ln 2}\int_0^\infty \frac{1}{1+x}\exp(-\Psi x)\frac{\pi}{2M}\sum_{m=1}^{M}\sqrt{1-\phi_m^2} \\ \cdot \sqrt{\frac{\Phi[\Psi(x^2+x)-x\ln u]}{-\ln u(-\ln u+\Psi x)}}K_1\left(\sqrt{\frac{\Phi[\Psi(x^2+x)-x\ln u]}{-\ln u(-\ln u+\Psi x)}}\right)dx. \end{aligned} \tag{32}$$

Let $t = \exp(-\Psi x)$ be a new variable, (32) can be rewritten as

$$\begin{aligned} \mathscr{C}_{\mathrm{AF}} = \frac{\pi}{2M\ln 2}\sum_{m=1}^{M}\sqrt{1-\phi_m^2}\int_0^1 \frac{1}{\Psi+\ln(1/t)} \\ \cdot \sqrt{\frac{\Phi\ln(1/t)(\ln(1/t)-\ln u+\Psi)}{-\Psi\ln u(\ln(1/t)-\ln u)}}K_1 \\ \cdot \left(\sqrt{\frac{\Phi[\Psi(x^2+x)-x\ln u]}{-\Psi\ln u(\ln(1/t)-\ln u)}}\right)dt. \end{aligned} \tag{33}$$

Applying [39] (Eq. (25.4.30)), the integral in (33) is calculated as

$$\int_0^1 \frac{1}{\Psi + \ln(1/t)} \sqrt{\frac{\Phi \ln(1/t)(\ln(1/t) - \ln u + \Psi)}{-\Psi \ln u(\ln(1/t) - \ln u)}} K_1 \cdot \left(\sqrt{\frac{\Phi \ln(1/t)(\ln(1/t) - \ln u + \Psi)}{-\Psi \ln u(\ln(1/t) - \ln u)}} \right) dt = \frac{\pi}{2N} \sum_{n=1}^{N} \frac{\sqrt{1-\phi_n^2}}{\Psi - \ln v} \sqrt{\frac{\Phi \ln v(\ln u + \ln u - \Psi)}{\Psi \ln u(\ln u + \ln v)}} K_1 \cdot \left(\sqrt{\frac{\Phi \ln v(\ln u + \ln u - \Psi)}{\Psi \ln u(\ln u + \ln v)}} \right), \tag{34}$$

where N, ϕ_n, and v were defined in the theorem.

Replacing (34) into (33), we obtain the EC of the considered system with the AF protocol as (18).

For the DF protocol, the CDF of γ_{DF} (denoted by $F_{\mathrm{DF}}(x)$) is computed as

$$\begin{aligned} F_{\mathrm{DF}}(x) &= \Pr\{\gamma_{\mathrm{DF}} < x\} = \Pr\{\min(\gamma_{\mathrm{R}}, \gamma_{\mathrm{D}}) < x\} \\ &= 1 - \Pr\{\gamma_{\mathrm{R}} > x, \gamma_{\mathrm{D}} > x\}. \end{aligned} \tag{35}$$

Substituting γ_{R} and γ_{D} in (13) and (14) into (35), we have

$$\begin{aligned} F_{\mathrm{DF}}(x) &= 1 - \Pr\left\{ \frac{|h_{\mathrm{SR}}|^2 P_{\mathrm{S}}}{\sigma_{\mathrm{RSI}}^2 + \sigma_{\mathrm{R}}^2} > x, \frac{|h_{\mathrm{SR}}|^2 |h_{\mathrm{RD}}|^2 \eta\alpha P_{\mathrm{S}}}{\sigma_{\mathrm{D}}^2(1-\alpha)} > x \right\} \\ &= 1 - \Pr\left\{ |h_{\mathrm{SR}}|^2 > \frac{x(\sigma_{\mathrm{RSI}}^2 + \sigma_{\mathrm{R}}^2)}{P_{\mathrm{S}}}, |h_{\mathrm{RD}}|^2 > \frac{x\sigma_{\mathrm{D}}^2(1-\alpha)}{|h_{\mathrm{SR}}|^2 \eta\alpha P_{\mathrm{S}}} \right\} \\ &= 1 - \left(1 - \Pr\left\{ |\mathrm{v}|^2 \le \frac{x\sigma_{\mathrm{D}}^2(1-\alpha)}{|h_{\mathrm{SR}}|^2 \eta\alpha P_{\mathrm{S}}} \Big|_{|h_{\mathrm{SR}}|^2 > \left(x\left(\sigma_{\mathrm{RSI}}^2 + \sigma_{\mathrm{R}}^2\right)/P_{\mathrm{S}}\right)} \right\} \right). \end{aligned} \tag{36}$$

Using the conditional probability [44], (36) can be expressed as

$$F_{\mathrm{DF}}(x) = 1 - \int_0^\infty \left(1 - F_{|h_{\mathrm{RD}}|^2}\left(\frac{x\sigma_{\mathrm{D}}^2(1-\alpha)}{|h_{\mathrm{SR}}|^2 \eta\alpha P_{\mathrm{S}}} \right) \right) f_{|h_{\mathrm{SR}}|^2}\left(y + \frac{x(\sigma_{\mathrm{RSI}}^2 + \sigma_{\mathrm{R}}^2)}{P_{\mathrm{S}}} \right) dy, \tag{37}$$

where $y = |h_{\mathrm{SR}}|^2 - (x(\sigma_{\mathrm{RSI}}^2 + \sigma_{\mathrm{R}}^2)/P_{\mathrm{S}})$.

Applying (25) and (26), (37) becomes

$$\begin{aligned} F_{\mathrm{DF}}(x) &= 1 - \int_0^\infty \sqrt{\frac{4x\sigma_{\mathrm{D}}^2(1-\alpha)}{\left(y + \left(x\left(\sigma_{\mathrm{RSI}}^2 + \sigma_{\mathrm{R}}^2\right)/P_{\mathrm{S}}\right)\right)\eta\alpha P_{\mathrm{S}}}} K_1 \cdot \left(\sqrt{\frac{4x\sigma_{\mathrm{D}}^2(1-\alpha)}{\left(y + \left(x\left(\sigma_{\mathrm{RSI}}^2 + \sigma_{\mathrm{R}}^2\right)/P_{\mathrm{S}}\right)\right)\eta\alpha P_{\mathrm{S}}}} \right) \exp \cdot \left(-y - \frac{x\left(\sigma_{\mathrm{RSI}}^2 + \sigma_{\mathrm{R}}^2\right)}{P_{\mathrm{S}}} \right) dy \\ &= 1 - \int_0^\infty \sqrt{\frac{\Phi x}{y + \Psi x}} K_1 \left(\sqrt{\frac{\Phi x}{y + \Psi x}} \right) \exp(-y - \Psi x) dy z \\ &= 1 - \exp(-\Psi x) \int_0^\infty \sqrt{\frac{\Phi x}{y + \Psi x}} K_1 \left(\sqrt{\frac{\Phi x}{y + \Psi x}} \right) \exp(-y) dy. \end{aligned} \tag{38}$$

Applying all steps used for the AF protocol such as changing variable $z = \exp(-y)$ and using [39] (Eq. (25.4.30)), we can obtain the CDF of the considered system with the DF protocol as

$$F_{\mathrm{DF}}(x) = 1 - \frac{\pi}{2M} \exp(-\Psi x) \sum_{m=1}^{M} \sqrt{1-\phi_m^2} \sqrt{\frac{\Phi x}{\Psi x - \ln u}} K_1 \cdot \left(\sqrt{\frac{\Phi x}{\Psi x - \ln u}} \right). \tag{39}$$

Then, substituting (39) into (17) and applying similar transformations used for the AF protocol, we obtain the EC of the considered system with the DF protocol as (19). The proof is complete.

4. Numerical Results and Discussions

In this section, the mathematical expressions in the previous section are used to evaluate the ECs of the considered FD-EH-V2V relay system with AF/DF protocols. The effect of several system parameters such as the RSI level, the average transmission power, the time switching ratio, and the cascade Rayleigh fading is investigated to provide the system deployment guidelines in practice. All mathematical expressions are validated through Monte-Carlo simulations. In particular, we use the MATLAB simulator to obtain the simulation results. To generate a cascade Rayleigh fading channel, we generate two independent Rayleigh fading channels and then multiply these two channels. To realize the ECs of the HD-EH-V2V relay systems, we set the RSI level $k = 0$ in the obtained EC expressions of the FD-EH-V2V relay systems and divide the results by two because HD-EH-V2V relay systems need two time slots to transmit signal from S to D via R. In all scenarios, we set $\sigma_{\mathrm{R}}^2 = \sigma_{\mathrm{D}}^2 = \sigma^2$, the energy harvesting efficiency $\eta = 0.85$, and the complexity-accuracy trade-off parameters $M = N = 20$. In addition, the average transmission power is calculated as $\mathrm{SNR} = P_{\mathrm{S}}/\sigma^2$. Furthermore, ECs of the considered system are compared with those in the case of Rayleigh fading channel and HD transmission mode to demonstrate the benefits of the FD technique and the impacts of the RSI and cascade Rayleigh fading. For the sake of redoing the simulation easily by other researchers, we summarize the parameter settings for evaluating the system performance in Table 1.

Figure 3 illustrates the ECs of the considered FD-EH-V2V relay system versus the average SNR for different values of the RSI level, i.e., $k = -30, -20$, and -10 dB. The time switching ratio is $\alpha = 0.5$. We use (18) and (19) in the theorem to plot the ECs of the considered FD-EH-V2V relay system with AF and DF protocols. In Figure 3, the ECs of the

Table 1: Parameter settings for evaluating the system performance.

Notation	Description	Fixed value	Varying range
SNR	Signal-to-noise ratio	40 dB	10, 20, 30, 50 dB; 0~50 dB
σ^2	Variance of Gaussian noise	1	None
η	Energy harvesting efficiency	0.85	None
α	Time switching ratio	0.5	0.1~0.9
k	RSI level	-20 dB	-10, -30 dB; 0~0.2
M, N	Trade-off parameters	20	None

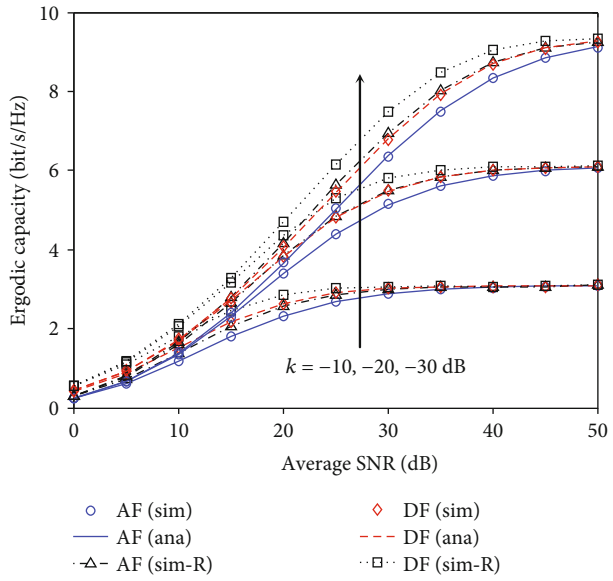

Figure 3: The ECs of the considered FD-EH-V2V relay system for different values of the RSI level, $k = -30, -20$, and -10 dB; $\alpha = 0.5$.

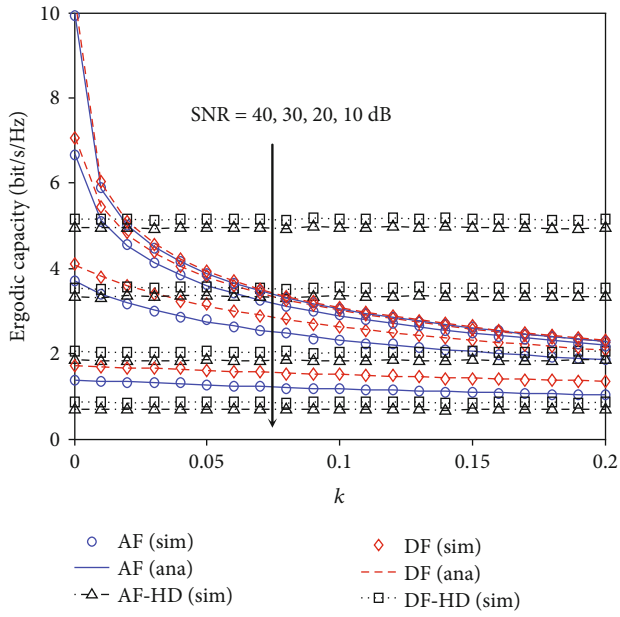

Figure 4: The impact of RSI on the ECs of the considered FD-EH-V2V relay system for different average transmission power, SNR = 10, 20, 30, and 40 dB; $\alpha = 0.5$.

FD-EH system over Rayleigh fading channels are denoted by "Sim-R." As shown in Figure 3, the cascade Rayleigh fading reduces the ECs compared with the Rayleigh fading, especially in low SNR regime and low RSI level. Particularly, when RSI is low, i.e., $k = -30$ dB, the ECs of the considered system are 0.2 bit/s/Hz lower than those in the case of Rayleigh fading for both AF and DF protocols at SNR = 30 dB. However, all ECs approximate 9 bit/s/Hz at SNR = 50 dB. With higher RSI levels, i.e., $k = -20$ and -10 dB, all ECs reach the capacity ceilings at SNR = 40 dB and 50 dB for the case $k = -10$ dB and $k = -20$ dB, respectively. In these two cases, the ECs only reach 3.1 and 6 bit/s/Hz for $k = -10$ dB and $k = -20$ dB, respectively. These features indicate a strong impact of RSI on the ECs of the considered FD-EH-V2V relay system. On the other hand, the ECs with the DF protocol are always higher than those with the AF protocol. This result is reasonable because AF amplifies not only noise but also the RSI.

Figure 4 investigates the effect of the RSI on the ECs of the considered FD-EH-V2V relay system for different average transmission power, i.e., SNR = 10, 20, 30, and 40 dB. We also provide the ECs of the considered system with HD transmission mode to clearly show the impact of RSI and the benefit of FD transmission mode. It is evident from Figure 4 that the effect of RSI is significant for high SNRs. Specifically, when self-interference is obliterated ($k = 0$), the ECs of the FD-EH-V2V relay system are two times higher than the ECs of the HD-EH-V2V relay system. When k increases, the ECs of the considered FD-EH-V2V relay system decrease. In particular, the ECs of the FD-EH-V2V relay system are always higher than ECs of the HD-EH-V2V relay system for low SNRs, i.e., SNR = 10 and 20 dB. However, for higher SNRs, i.e., SNR = 30 and 40 dB, the ECs of the FD-EH-V2V relay system are higher or lower than the ECs of the HD-EH-V2V relay system. For example, the ECs of the FD-EH-V2V relay system are higher than the ECs of the HD-EH-V2V relay system when k ranges from 0 to 0.07 and SNR = 30 dB. When $k > 0.07$, the ECs of the FD-EH-V2V relay system are lower than the ECs of the HD-EH-V2V relay system. With higher SNR, i.e., SNR = 40 dB, the ECs of the FD-EH-V2V relay system are only higher than those of the HD-EH-V2V relay system when $k < 0.03$. Therefore, depending on the measured and experimented RSI levels in practice, we can select FD or HD transmission mode to obtain high system capacity.

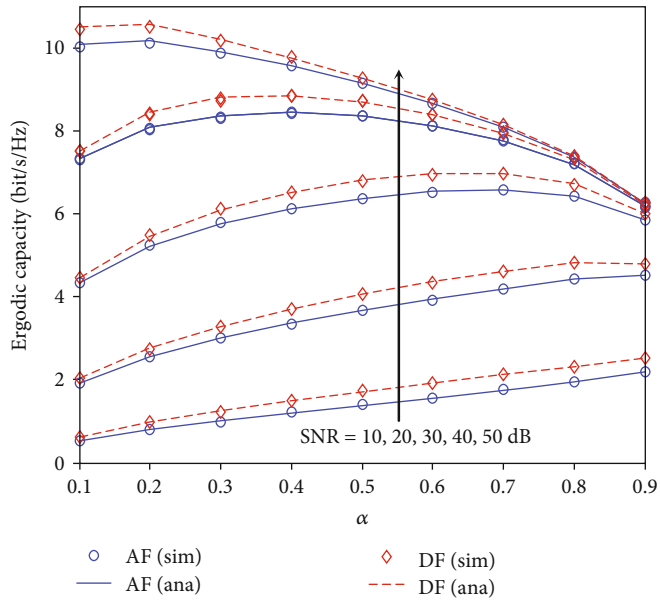

FIGURE 5: The ECs of the considered FD-EH-V2V relay system versus the time switching ratio α for different SNRs, $k = -30$ dB.

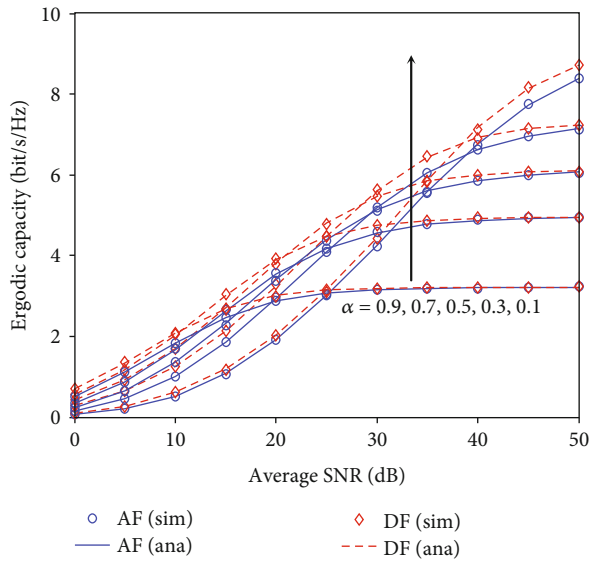

FIGURE 6: The ECs of the considered FD-EH-V2V relay system versus the average SNR for different values of time switching ratio, $k = -20$ dB.

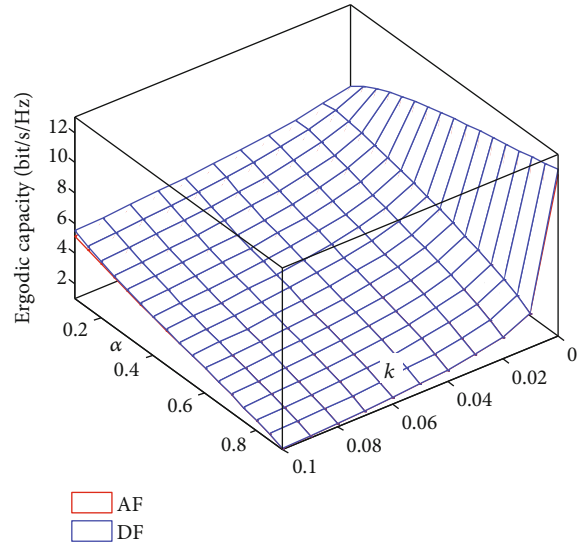

FIGURE 7: The joint impacts of the RSI level k and the time switching ratio α on the ECs of the considered FD-EH-V2V relay system.

Figure 5 shows the ECs of the considered FD-EH-V2V relay system versus the time switching ratio α for different SNRs, e.g., SNR = 10, 20, 30, 40, and 50 dB. The RSI level is $k = -30$ dB. As observed in Figure 5, it is obvious that the ECs of the considered FD-EH-V2V relay system closely depend on α. When SNR is small, i.e., SNR = 10 and 20 dB, the ECs increase with α. It is because small SNR means low transmission power of S; thus, R needs more time for EH to have enough signal transmission power. However, when SNR is higher, i.e., SNR = 30, 40, and 50 dB, the ECs firstly increase and then decrease when α gets higher. Specifically, for SNR = 30 dB and SNR = 40 dB, ECs are maximal when $\alpha = 0.7$ and $\alpha = 0.4$, respectively, for both AF and DF protocols. If the transmission power of S continues to increase, i.e., SNR = 50 dB, ECs are maximal when $\alpha = 0.2$. Therefore, based on the transmission power of S, the optimal α can be used to obtain the peak ECs of the considered FD-EH-V2V relay system.

To understand the relationship between the average transmission power of source and the time switching ratio α, we plot the ECs of the considered FD-EH-V2V relay system versus the average SNR for various time switching ratio, $\alpha = 0.1,0.3,0.5,0.7,0.9$, as shown in Figure 6. We can see that, in a low SNR regime, i.e., SNR < 20 dB, the EC of the case $\alpha = 0.7$ is the best while the EC of the case $\alpha = 0.1$ is the worst. However, for higher SNR range, 20 < SNR < 40 dB, the EC of the case $\alpha = 0.3$ is the best while the EC of the case $\alpha = 0.9$ is

the worst. If the average SNR still increases, i.e., SNR > 40 dB, the EC of the case $\alpha = 0.1$ is the best while the EC of the case $\alpha = 0.9$ is still the worst. To sum up, low SNR leads to a high α and vice versa.

The joint and cross impacts of the RSI level k and the time switching ratio α on the ECs of the considered FD-EH-V2V relay system are illustrated in Figure 7, where the average SNR is set as SNR = 40 dB. Similar to the ECs in Figure 5, with a certain value of k, there is an optimal α that maximizes ECs of AF/DF protocols. In particular, when $k = 0.01$, the ECs reach the maximum of 6.9 and 7.3 bit/s/Hz for AF and DF protocols, respectively, at $\alpha = 0.15$. However, with a higher value of k, the ECs are the highest when $\alpha = 0.1$. In other words, for k ranges from 0.02 to 0.2, ECs of AF/DF protocols decrease when α increases. Surprisingly, in the case of perfect SIC ($k = 0$), the ECs increase when α increases. As a result, besides reducing the ECs of the considered FD-EH-V2V relay system, the RSI also influences the optimal ECs. Therefore, for choosing an optimal α that maximizes the ECs of the considered system, it is necessary to know the RSI level and the average transmission power of the source before deploying this system in practice.

5. Conclusion

Applying FD and EH techniques are inevitable for future wireless networks, especially for V2V communication systems, because of the big advantages of these techniques. Therefore, in this paper, we evaluate the ergodic capacities of an FD-EH-V2V relay system with both AF and DF protocols under the impact of RSI and cascade Rayleigh fading channel. We mathematically derive the exact closed-form expressions of the EC of both AF and DF protocols. Numerical results reveal that the EC of the DF protocol is slightly higher than that of the AF one. Also, the cascade Rayleigh fading reduces the ECs of the considered system compared with the traditional Rayleigh fading. Furthermore, the ECs of the considered system are compared with those in the case of HD transmission mode to demonstrate the benefit of the FD technique. We also observe that, based on the RSI level and the source's average transmission power, we can choose an optimal time switching ratio to maximize the ECs of the considered FD-EH-V2V relay system.

Data Availability

The data used to support the findings of this study are available from the corresponding author upon request.

Conflicts of Interest

The authors declare that they have no conflicts of interest.

References

[1] Y. Zhao, "A survey of 6G wireless communications: emerging technologies," 2020, http://arxiv.org/abs/2004.08549.

[2] M. Babaei, U. Aygolu, M. Basaran, and L. Durak-Ata, "BER performance of full-duplex cognitive radio network with non-linear energy harvesting," *IEEE Transactions on Green Communications and Networking*, vol. 4, no. 2, pp. 448–460, 2020.

[3] Q.-V. Pham, F. Fang, V. N. Ha et al., "A survey of multi-access edge computing in 5G and beyond: fundamentals, technology integration, and state-of-the-art," *IEEE Access*, vol. 8, pp. 116974–117017, 2020.

[4] B. Clerckx, R. Zhang, R. Schober, D. W. K. Ng, D. I. Kim, and H. V. Poor, "Fundamentals of wireless information and power transfer: from RF energy harvester models to signal and system designs," *IEEE Journal on Selected Areas in Communications*, vol. 37, no. 1, pp. 4–33, 2018.

[5] H. H. M. Tam, H. D. Tuan, A. A. Nasir, T. Q. Duong, and H. V. Poor, "MIMO energy harvesting in full-duplex multi-user networks," *IEEE Transactionson Wireless Communications*, vol. 16, no. 5, pp. 3282–3297, 2017.

[6] A. H. Gazestani, S. A. Ghorashi, B. Mousavinasab, and M. Shikh-Bahaei, "A survey on implementation and applications of full duplex wireless communications," *Physical Communication*, vol. 34, pp. 121–134, 2019.

[7] Y. Deng, K. J. Kim, T. Q. Duong, M. Elkashlan, G. K. Karagiannidis, and A. Nallanathan, "Full-duplex spectrum sharing in cooperative single carrier systems," *IEEE Transactions on Cognitive Communications and Networking*, vol. 2, no. 1, pp. 68–82, 2016.

[8] B. C. Nguyen, X. N. Tran, and L. T. Dung, "On the performance of roadside unit-assisted energy harvesting full-duplex amplify-and-forward vehicle-to-vehicle relay systems," *AEU-International Journal of Electronics and Communications*, vol. 123, article 153289, 2020.

[9] N.-P. Nguyen, C. Kundu, H. Q. Ngo, T. Q. Duong, and B. Canberk, "Secure full-duplex small-cell networks in a spectrum sharing environment," *IEEE Access*, vol. 4, pp. 3087–3099, 2016.

[10] B. C. Nguyen, N. N. Thang, T. M. Hoang, and L. T. Dung, "Analysis of outage probability and throughput for energy harvesting full-duplex decode-and-forward vehicle-to-vehicle relay system," *Wireless Communications and Mobile Computing*, vol. 2020, Article ID 3539450, 10 pages, 2020.

[11] Y. Alsaba, C. Y. Leow, and S. K. A. Rahim, "Full-duplex cooperative non-orthogonal multiple access with beamforming and energy harvesting," *IEEE Access*, vol. 6, pp. 19726–19738, 2018.

[12] A. Koc, I. Altunbas, and E. Basar, "Two-way full-duplex spatial modulation systems with wireless powered AF relaying," *IEEE Wireless Communications Letters*, vol. 7, no. 3, pp. 444–447, 2018.

[13] C. Guo, L. Zhao, C. Feng, Z. Ding, and H.-H. Chen, "Energy harvesting enabled NOMA systems with full-duplex relaying," *IEEE Transactions on Vehicular Technology*, vol. 68, no. 7, pp. 7179–7183, 2019.

[14] T. M. Hoang, V. Van Son, N. C. Dinh, and P. T. Hiep, "Optimizing duration of energy harvesting for downlink NOMA full-duplex over Nakagami-m fading channel," *AEU-International Journal of Electronics and Communications*, vol. 95, pp. 199–206, 2018.

[15] C. Li, Z. Chen, Y. Wang, Y. Yao, and B. Xia, "Outage analysis of the full-duplex decode-and-forward two-way relay system," *IEEE Transactions on Vehicular Technology*, vol. 66, no. 5, pp. 4073–4086, 2017.

[16] B. C. Nguyen, X. N. Tran, D. T. Tran, and L. T. Dung, "Full-duplex amplify-and-forward relay system with direct link:

performance analysis and optimization," *Physical Communication*, vol. 37, article 100888, 2019.

[17] X.-T. Doan, N.-P. Nguyen, C. Yin, D. B. Da Costa, and T. Q. Duong, "Cognitive full-duplex relay networks under the peak interference power constraint of multiple primary users," *EURASIP Journal on Wireless Communications and Networking*, vol. 2017, no. 1, 2017.

[18] V.-D. Nguyen, T. Q. Duong, H. D. Tuan, O.-S. Shin, and H. V. Poor, "Spectral and energy efficiencies in full-duplex wireless information and power transfer," *IEEE Transactions on Communications*, vol. 65, no. 5, pp. 2220–2233, 2017.

[19] D. H. Chen and Y. C. He, "Full-duplex secure communications in cellular networks with downlink wireless power transfer," *IEEE Transactions on Communications*, vol. 66, no. 1, pp. 265–277, 2018.

[20] C. Campolo, A. Molinaro, A. O. Berthet, and A. Vinel, "Full-duplex radios for vehicular communications," *IEEE Communications Magazine*, vol. 55, no. 6, pp. 182–189, 2017.

[21] M. Yang, S.-W. Jeon, and D. K. Kim, "Interference management for in-band full-duplex vehicular access networks," *IEEE Transactions on Vehicular Technology*, vol. 67, no. 2, pp. 1820–1824, 2018.

[22] Y. Ai, M. Cheffena, A. Mathur, and H. Lei, "On physical layer security of double Rayleigh fading channels for vehicular communications," *IEEE Wireless Communications Letters*, vol. 7, no. 6, pp. 1038–1041, 2018.

[23] R. Atallah, M. Khabbaz, and C. Assi, "Energy harvesting in vehicular networks: a contemporary survey," *IEEE Wireless Communications*, vol. 23, no. 2, pp. 70–77, 2016.

[24] A. Sabharwal, P. Schniter, D. Guo, D. W. Bliss, S. Rangarajan, and R. Wichman, "In-band full-duplex wireless: challenges and opportunities," *IEEE Journal on Selected Areas in Communications*, vol. 32, no. 9, pp. 1637–1652, 2014.

[25] T. Riihonen, S. Werner, and R. Wichman, "Mitigation of loopback self-interference in full-duplex MIMO relays," *IEEE Transactions on Signal Processing*, vol. 59, no. 12, pp. 5983–5993, 2011.

[26] E. Everett, A. Sahai, and A. Sabharwal, "Passive self-interference suppression for full-duplex infrastructure nodes," *IEEE Transactions on Wireless Communications*, vol. 13, no. 2, pp. 680–694, 2014.

[27] Q. N. Le, V. N. Q. Bao, and B. An, "Full-duplex distributed switch-and-stay energy harvesting selection relaying networks with imperfect CSI: design and outage analysis," *Journal of Communications and Networks*, vol. 20, no. 1, pp. 29–46, 2018.

[28] C. Zhong, H. A. Suraweera, G. Zheng, I. Krikidis, and Z. Zhang, "Wireless information and power transfer with full duplex relaying," *IEEE Transactions on Communications*, vol. 62, no. 10, pp. 3447–3461, 2014.

[29] X. Lin, G. Sharma, R. R. Mazumdar, and N. B. Shroff, "Degenerate delay-capacity tradeoffs in ad-hoc networks with Brownian mobility," *IEEE Transactions on Information Theory*, vol. 52, no. 6, pp. 2777–2784, 2006.

[30] G. Sharma, R. Mazumdar, and N. Shroff, "Delay and capacity trade-offs in mobile ad hoc networks: a global perspective," *IEEE/ACM Transactions on Networking*, vol. 15, no. 5, pp. 981–992, 2007.

[31] D. Tian and V. C. Leung, "Analysis of broadcasting delays in vehicular ad hoc networks," *Wireless Communications and Mobile Computing*, vol. 11, no. 11, pp. 1433–1445, 2011.

[32] J. Salo, H. M. El-Sallabi, and P. Vainikainen, "Statistical analysis of the multiple scattering radio channel," *IEEE Transactions on Antennas and Propagation*, vol. 54, no. 11, pp. 3114–3124, 2006.

[33] I. Kovacs, *Radio channel characterisation for private mobile radio systems - mobile-to-mobile radio link investigations: mobile-to-mobile radio link investigations*, Ph.D. dissertation, 2002.

[34] B. C. Nguyen, X. N. Tran, T. M. Hoang, and L. T. Dung, "Performance analysis of full-duplex vehicle-to-vehicle relay system over double-Rayleigh fading channels," *Mobile Networks and Applications*, vol. 25, no. 1, pp. 363–372, 2020.

[35] T. T. Duy, G. C. Alexandropoulos, V. T. Tung, V. N. Son, and T. Q. Duong, "Outage performance of cognitive cooperative networks with relay selection over double-Rayleigh fading channels," *IET Communications*, vol. 10, no. 1, pp. 57–64, 2016.

[36] B. C. Nguyen, T. M. Hoang, P. T. Tran, and T. N. Nguyen, "Outage probability of NOMA system with wireless power transfer at source and full-duplex relay," *AEU - International Journal of Electronics and Communications*, vol. 116, article 152957, 2020.

[37] D. Bharadia, E. McMilin, and S. Katti, "Full duplex radios," in *SIGCOMM '13: Proceedings of the ACM SIGCOMM 2013 conference on SIGCOMM*, pp. 375–386, New York, NY, USA, August 2013.

[38] L. Van Nguyen, B. C. Nguyen, X. N. Tran, and L. T. Dung, "Transmit antenna selection for full-duplex spatial modulation multiple-input multiple-output system," *IEEE Systems Journal*, vol. 14, no. 4, pp. 4777–4785, 2020.

[39] M. Abramowitz and I. A. Stegun, *Handbook of Mathematical Functions with Formulas, Graphs, and Mathematical Tables, vol. 9*, Dover, New York, NY, USA, 1972.

[40] A. Jeffrey and D. Zwillinger, *Table of Integrals, Series, and Products*, Academic Press, 2007.

[41] B. C. Nguyen, T. M. Hoang, and L. T. Dung, "Performance analysis of vehicle-to-vehicle communication with full-duplex amplify-and-forward relayover double-Rayleigh fading channels," *Vehicular Communications*, vol. 19, pp. 1–9, 2019.

[42] I. Z. Kovacs, P. C. F. Eggers, K. Olesen, and L. G. Petersen, "Investigations of outdoor-to-indoor mobile-to-mobile radio communication channels," in *Proceedings IEEE 56th Vehicular Technology Conference*, pp. 430–434, Vancouver, BC, Canada, September 2002.

[43] A. Pandey and S. Yadav, "Secrecy analysis of cooperative vehicular relaying networks over double-Rayleigh fading channels," *Wireless Personal Communications*, vol. 114, no. 3, pp. 2733–2753, 2020.

[44] A. Leon-Garcia and A. Leon-Garcia, *Probability, Statistics, and Random Processes for Electrical Engineering*, Pearson/Prentice Hall, UpperSaddle River, NJ, USA, 3rd edition, 2008.